Uncertainties in the estimation of local peak pressures on low-rise buildings by using the Gumbel distribution fitting approach

Gavanski, Eri; Gurley, K.R.; Kopp, Gregory

DOI:
10.1061/(ASCE)ST.1943-541X.0001556

Document Version
Peer reviewed version

Citation for published version (Harvard):
Gavanski, E, Gurley, KR & Kopp, G 2016, 'Uncertainties in the estimation of local peak pressures on low-rise buildings by using the Gumbel distribution fitting approach', *Journal of Structural Engineering (United States)*, vol. 142, no. 11. https://doi.org/10.1061/(ASCE)ST.1943-541X.0001556

Uncertainties in the estimation of local peak pressures on low-rise buildings by Gumbel-fitting approach

Eri Gavanski, Ph. D.[1], Kurtis R. Gurley, Ph. D.[2*], Gregory A. Kopp, Ph. D.[3]

[1] Disaster Prevention Research Institute, Kyoto University, Uji, Kyoto, Japan, 611-0011
[2] Department of Civil and Coastal Engineering, University of Florida, P.O. Box 116580, Gainesville, FL 326611-6580, USA
[3] Boundary Layer Wind Tunnel Laboratory, Faculty of Engineering, University of Western Ontario, London, ON, Canada, N6A 5B9

Abstract

The lack of a standard accepted method to estimate local peak pressure coefficients from wind tunnel data can lead to inconsistent definitions and interpretations, particularly since cost and time constraints associated with wind tunnel tests of low-rise buildings necessitate that relatively short (equivalent full-scale) test durations be used. This paper focuses on a Gumbel distribution fitting method widely used in practice. Since the sources of uncertainty on estimated peaks include the use of short duration records (in practice) and the assumption that the observed peaks from wind tunnel pressure data are Gumbel distributed, this is quantified in detail in terms of the parameters determining the required minimum record length. It is shown that 15 observed peaks can lead to local peak pressure estimates with adequate precision for many design scenarios. However, the conversion of peak coefficients from a short duration to those of a longer duration requires an increase in the number of observed peaks to maintain precision.

* Author to whom correspondence should be addressed. Email: gavanski.eri.7a@kyoto-u.ac.jp; phone: +81-774-38-4169; fax: +81-774-38-4170.
E-mail addresses: gavanski.eri.7a@kyoto-u.ac.jp (E. Gavanski), kgurl@ce.ufl.edu (K.R. Gurley), gakopp@uwo.ca (G.A. Kopp).

INTRODUCTION

There have been many studies that present estimates of peak pressure coefficients, Cp_{pk}, for the design of building components and cladding (C&C) on low-rise structures (e.g., Davenport 1964; Cook and Mayne 1979; Stathopoulos 1979; Dagliesh and Templin 1980; Sockel 1980; Peterka, 1983; Kasperski 1997; Holmes and Moriarty 1999; Sadek and Simiu 2002; Holmes and Cochran 2003; Kasperski 2003). Considerable variations exist regarding the definition of and methodologies to estimate Cp_{pk}. These variations infiltrate the wind load design standards used around the world. Although there is a common thread in the use of scale models with boundary layer wind tunnels as the basis for Cp_{pk} development, the lack of a standard accepted methodology and the dearth of clarity in the supporting documentation inhibits repeatability, transparency, and the identification of best practices.

This paper addresses these issues in two parts. A historical and current-state-of-practice review is conducted via exhaustive literature review to identify the evolution of and geographic differences in the estimation of Cp_{pk}. This is followed by an analysis of a surface-pressure dataset from a low-rise residential-building model. Due to its prevalence, the analysis focuses on fitting a Gumbel distribution to observed peaks. A parametric study is conducted to identify the uncertainties associated with the common use of relatively short duration records as well as the selected Cp_{pk} estimation parameters. The duration in which a single peak is observed (t_{pk_g}) and the number of peaks observed (n_{pk_g}) are varied within a given fixed record length ($t_{total} = n_{pk\_g} \times t_{pk\_g}$) to determine combinations with acceptable uncertainty. All the nomenclature used in the current study is summarized in the notation list.

CURRENT AND HISTORICAL PRACTICE

A review of more than 150 journal and conference papers identified six different peak estimation methods: (1) single worst peak, which uses the single extreme value recorded during a sampling period; (2) an ensemble-average of several maxima (minima) taken from equal-length segments; (3) Gumbel fitting method, which uses several maxima (minima) to determine the parameters and estimates the peak corresponding to a certain fractile level ($F_{\text{pk\_frac}}$); (4) Cook-Mayne method, which is discussed further below; (5) translation method, which utilizes a full time series rather than observed peaks to obtain a peak Cumulative Distribution Function (CDF); and (6) peak factor method, which estimates peak value as the sum of the mean value plus the standard deviation multiplied by a peak factor. The Gumbel fitting method is similar to Cook-Mayne method, with the peak fractile level fixed for the latter.

The review reveals that Cp_{pk} estimation methods have varied both by era and region. Table 1 shows the number of papers employing the different peak estimation methods stratified by decadal eras. The simple worst peak method was dominant through the 1980s, after which ensemble-average and Gumbel fitting methods began to emerge. The translation and peak factor methods were proposed in the early 2000s, while the peak observation-based and the Gumbel-fitting methods continued to receive the bulk of attention. In the current era, peak factor and translation methods are nominally increasing in use, but simple worst, ensemble-average, and Cook-Mayne methods are still more frequent. Universities and research facilities that only recently began to participate in wind engineering tend to use the simple worst and peak factor methods, explaining its recent resurgence despite their lack of a statistical basis. It is also worth noting the recurring instance of papers that did not reveal the specific Cp_{pk} estimation methods used. Table 2 presents

71 the same data stratified by region, offering both the distribution of methods and the relative volume
72 of papers.

73 Beyond those described in Tables 1 and 2, there are several other peak estimation methods in
74 the literature, such as fitting the peak to the Type III Extreme value distribution (Kasperski 2003),
75 the Generalized Pareto distribution with peaks over threshold data (Simiu and Heckert 1996;
76 Holmes and Morality 1999; Holmes and Cochran 2003), and the methods suggested for wind
77 velocity estimation (e.g., Method of Independent Storms by Harris (2009) and others). Although
78 these methods may be able to estimate peaks with higher accuracy, and are based on sound theory,
79 the methods listed in Tables 1 and 2 appear to be preferred due to simplicity and the requirements
80 of relatively shorter sampling times.

81 Table 3 summarizes whether design codes explicitly define Cp_{pk} and the methodology to
82 determine it, and whether documentation is referenced. Only ISO 4354 (ISO 2009) clearly defines
83 Cp_{pk} and its estimation method. Australia/New Zealand and Japan have published a user's manual
84 wherein the recommended estimation method is explained, and this seems to be helping to reduce
85 the variability of employed peak estimation methods in this region (Table 2). For North and South
86 America, no recommendations are made, nor the calculation method provided. In Europe, the use
87 of Cook-Mayne method is dominant in the literature (Table 2). In the Eurocode, Cook-Mayne
88 method is employed for the calculation of structural design loads, but C&C loads appear to be
89 calculated using simple worst peaks (Geurts et al. 2001; Geurts et al. 2013).

90 The lack of a standard Cp_{pk} definition or estimation methodology presents obvious weaknesses
91 regarding repeatability, as different researchers/practitioners will produce different Cp_{pk} estimates
92 given an identical dataset. With respect to the Gumbel-fitting method, the required parameters are
93 the number of peaks ($n_{\mathrm{pk\_g}}$), sampling duration ($t_{\mathrm{pk\_g}}$), and peak fractile level ($F_{\mathrm{pk\_frac}}$) that defines

Cp_{pk}. Fig. 1 shows the lack of consistency among studies that use the Gumbel-fitting method. This is, in part at least, attributable to the fact that the averaging period for the peak wind speed differs regionally. Table 3 and Fig. 1 also indicate that in some codes and manuals parameters are proposed as a range instead of a single value. For example, the Cook-Mayne method is based on the Gumbel-fitting approach to calculate its parameters with the Lieblein BLUE method, using (generally) 16 maximal (minimal) values (n_{pk_g}) whose evaluation time is between 10 min to 60 min in full-scale (t_{pk_g}), with 78% of peak fractile level (F_{pk_frac}), with a conversion to change the evaluation time to a longer one (Cook 1982; 1985). Similarly, ISO 4354 (ISO 2009) Annex D provides an equation (D.1) to estimate Cp_{pk} from wind tunnel data using the assumption that the peaks follow a Gumbel distribution. The mean and weighted root mean square (rms) values of a series of sequential peaks, each observed over a duration of t_{pk_g} = 60 min, are added to provide the Cp_{pk} defined as the 80% fractile corresponding to a reference period of 60 min. ISO 4354 also provides an equation (D.3) to utilize peaks observed from a duration of t_{pk_g} = 10 min to estimate the 60-min Cp_{pk} defined at the 80% fractile. Thus, ISO 4354 provides the t_{pk_g} and F_{pk_frac}. The required number of peaks (n_{pk_g}) to determine the mean and rms in equation D.1 or D.3 influences the uncertainty of the Cp_{pk} estimate, but is not specified.

STUDY OBJECTIVES

The objective of this study is to quantify, via a parametric study, the uncertainties associated with the Gumbel-fitting method to estimate Cp_{pk}, and the estimated peak will be denoted as Cp_{pk_g} for clarity. The Gumbel-fitting method is selected due to its wide use in practice, its simplicity, and its advantages over single or ensemble-averaged peak methods with respect to stability and the ability to select a target fractile. The accuracy of the method has been demonstrated relative to other methods (e.g., Harris 2001; Kasperski 2009; Peng et al. 2014). The current study focuses on

low-rise buildings because the relatively large model scales used in such studies lead to relatively long sampling durations. The parametric study is conducted within the context of the relatively short test durations (equivalent full scale durations of 15-20 minutes per wind direction) typically employed for low-rise wind tunnel testing in practice.

Long (30-hr equivalent full scale) wind-tunnel pressure records were collected on a 1/50 scale model of a residential structure. The full-scale companion structure is located on the Panhandle of Florida, for which measured pressure time histories were obtained during Hurricane Ivan in 2004 (Liu et al. 2009). The long duration wind tunnel data provide an empirical benchmark to compare the Cp_{pk} estimation using the Gumbel and ISO 4354 approaches applied to short duration segments of the long records. Quan et al. (2009) performed a study with similar goals regarding the identification of an acceptable t_{pk_g}, but utilized much shorter data records and did not quantify uncertainty originating from the variation of t_{pk_g}. In addition, the current study explicitly identifies the influence of t_{pk_g} and n_{pk_g} on the accuracy and precision of Cp_{pk_g}, providing practitioners with guidance regarding the selection of Cp_{pk} estimation parameters within the framework of uncertainty bounds.

WIND TUNNEL TESTING AND SELECTION OF TAPS FOR ANALYSIS

The wind tunnel experiments were conducted in Boundary Layer Wind Tunnel II at the University of Western Ontario (UWO). A single-story residential house was modeled at a scale of 1/50 and placed in suburban terrain exposure (z_0=0.23 m). Details can be found in Kopp and Gavanski (2010). The surface pressures acting at each tap on the roof were measured at the average reference wind speed of V_{ref} (14.5 m/s), and re-referenced to mean roof height (4.3 m). A sampling rate of 400 Hz for 3 hours (model scale) was used. Assuming a full-scale wind speed at 10 m height in suburban terrain (z_0=0.23 m) of 32 m/s (velocity scale = 1/5), the sampled data are equivalent to

30-hr in full scale (time scale = 1/10) at a sampling rate of 40 Hz. The pressure coefficient (*Cp*) data were digitally low-passed filtered at 200Hz (model scale). No corrections were made for missing energy in the wind tunnel data at large-scales/low-frequencies.

Fig. 2 shows the plan of the scale model with all tap locations marked. Since it is known that positive and negative pressures tend to have different characteristics in the upper tail of the distribution (Peterka and Cermak 1975), the current analysis focuses on the negative pressure because of the practical importance of roof loads. The methodology is first developed and applied to the four taps labelled in Fig. 2 to allow a detailed presentation of results. The methodology is then applied to all 493 taps. The approach wind direction isolated for analysis is identified in Fig. 2.

The four taps in Fig. 2 were chosen as a broad statistical representation of the available data with respect to the higher moments as quantified by the coefficients of skewness (*s*) and kurtosis (*k*). Fig. 3 presents a plot of *s* - *k* pairs for all 493 taps with the four taps in Fig. 2 highlighted. In order to examine the applicability of the suggested combination of t_{pk_g} and n_{pk_g} in terms of the non-Gaussian characteristics, the *s* - *k* pairs are stratified into four groups based on their kurtosis values ($10 \le k$, $5 \le k < 10$, $4 \le k < 5$, $k < 4$). The four selected taps include both mildly (Taps 1 and 2) and strongly non-Gaussian behavior (Taps 3 and 4). Table 4 provides summary statistics for each of the four selected taps.

METHODOLOGY AND RESULTS

Evaluation of the Gumbel model for approximating the peak CDF

The Cumulative distribution function (CDF) for the Gumbel distribution is

$$F_g = \exp\left[-\exp\left\{-\alpha(Cp - U)\right\}\right] \quad (1)$$

where α and U are the shape parameters to be selected based on the observed peaks.

The 30-hr long (full-scale) *Cp* time histories at each of the four selected taps were divided into 100 eighteen-minute segments and a peak (i.e., minima) was collected from each segment (n_{pk_g} =100 peaks with t_{pk_g} =18 min). These peaks were ordered from smallest to largest of their absolute values, and allocated the plotting position expressed as:

$$F_{emp} = i/(N+1) \quad (2)$$

where i is the rank of peak in ascendant order and N is the total number of peaks.

These empirical CDFs were compared with Gumbel CDF models, where the Gumbel parameters are calculated from the observed peaks using the Gumbel plot, Method of moments, Maximum likelihood, and the expanded generalized least-squares (GLS) method (i.e., Lieblein BLUE, Lieblein, 1974; Hong et al. 2013). The empirical and Gumbel-modeled CDFs are shown in Fig. 4. The horizontal gray lines indicate 50%, 80%, 90% and 99% fractile levels based on the empirical CDF. The approximation with a Gumbel distribution is generally acceptable. These results justify the use of the Gumbel-fitting approach, but also indicate that some error will be associated with the Gumbel assumption. The expanded GLS method will be used to select the Gumbel parameters if the number of peaks (n_{pk_g}) is 100 or less. Otherwise, maximum likelihood will be employed. The independence of observed peaks is addressed in the next section.

Effects of t_{pk_g} and n_{pk_g} on peak estimation uncertainty

Approach

The influence of duration (t_{pk_g}) and number of observed peaks (n_{pk_g}) on the accuracy and precision of a single peak pressure coefficient estimate (Cp_{pk_g}) is examined. This uncertainty quantification can be used to optimally select the appropriate t_{pk_g} and n_{pk_g} for a fixed wind tunnel testing time, or to select an appropriate wind tunnel test time ($t_{total} = t_{pk\_g} \times n_{pk\_g}$) based on a desired level of uncertainty.

The available stationary 30-hr (equivalent full-scale) wind-tunnel records from each of the four taps were divided into sub-records. A Gumbel model was fit to the observed peaks in a given sub-record using an assigned t_{pk_g} and n_{pk_g}. The 80% fractile was obtained from the Gumbel model to estimate Cp_{pk_g} in order to be consistent with ISO 4354 (2009). There is no standard, uniformly accepted or applied definition of an appropriate fractile, as evidenced in Table 3. Additionally, the majority of, but not all, studies in Figure 1 that did cite a specific definition used a 78% fractile. Hence, we have selected an 80% fractile as per ISO 4353. Given the lack of a standard however, the peak fractile level of 80% is somewhat arbitrary. A motivation for this work is to demonstrate that developing a standard is essential, and quantifying uncertainty regardless of peak definition, estimation method and duration is important. In this manner, multiple Cp_{pk_g} associated with a given t_{pk_g} and n_{pk_g} were created for each 30-hr record, providing a measure of the magnitude, accuracy and precision of Cp_{pk_g} as a function of the tap location, t_{pk_g} and n_{pk_g}.

In addition to the Cp_{pk_g}, an empirical peak value, Cp_{emp}, was calculated for each tap using observed peaks from the 30-hr record using an assigned t_{pk_g}. The corresponding probability was calculated using Eq. (2) and a peak fractile level of 80% was selected as Cp_{emp} in this study. Since more peaks can be obtained with smaller t_{pk_g} and a fixed wind tunnel data length (i.e., 30-hr), Cp_{emp} with smaller t_{pk_g} can be estimated with more peaks and, therefore, greater accuracy. In order to obtain a Cp_{emp} value that reflects only the difference of sampling length but not the number of peaks, a fixed number of observed peaks was employed for the calculation of Cp_{emp} regardless of t_{pk_g}. This was selected to be 60, which is the number of observed peaks obtained with t_{pk_g} =30 min.

208 With this approach, multiple 80% fractile peaks can be obtained for t_{pk_g} =2, 5, and 10 min. In
209 this case, the mean was treated as Cp_{emp}. For example, for t_{pk_g} =10 min, 180 observed peaks
210 (n_{pk_g} =180) can be obtained from the 30-hr record. Using the first set of 60 peaks with the
211 probability calculated from Eq. (2), a 80% fractile peak was calculated. This was repeated two
212 more times using the rest of the data and the mean of the three 80% fractile peaks was denoted as
213 Cp_{emp}. This empirical estimate, Cp_{emp}, is typically not available in practice, as wind tunnel
214 records are much shorter than 30 hrs. Thus, Cp_{emp} provides a unique point of comparison to
215 benchmark the accuracy and precision of the Gumbel-based Cp_{pk_g} estimated. Following Peng et
216 al. (2014), the standard error (S.E.) of the random variable Cp_{emp} was calculated at the fractile
217 level of 80% based on the Maritz-Jarrett method (Wilcox 2012). The S.E. was also calculated
218 using a fixed number of peaks (=60) regardless of t_{pk_g}, and their mean was denoted as S.E. for
219 the specific t_{pk_g}. It should be noted that Cp_{emp} +/- 3 S.E. represents a 99% confidence interval
220 against which to compare the Cp_{pk_g} (Krishnan 2006).
221 This study considers five values of t_{pk_g} and four values of n_{pk_g} at each of the four taps (Fig.
222 2). The length of the sub-record needed to create a single sample of Cp_{pk_g} (t_{total}) and the number
223 of Cp_{pk_g} samples produced for a given combination from the 30-hr record (n_{peak}) are provided in
224 Table 5.
225 The independence between peaks was examined by calculating the auto-correlation of the
226 individual *Cp* time series to determine a time lag that would imply independence between
227 sequential peaks. The results suggest that 40 sec (full scale) is a very conservative minimum time
228 lag to apply. Strictly speaking, the vanishing autocorrelation function does not prove independence
229 with the exception of Gaussian variables. However, the pressure peaks are a product of wind field
230 gusts, and the wind field is very nearly Gaussian. By this proxy argument and the very long (40

sec) time lag applied, it is reasonable to infer that peak gusts separated by a 40 sec time lag are independent. It was found that less than 10% of the sequential observed peaks had a time interval of less than 40 sec for the case of t_{pk_g} =2 min. Using t_{pk_g} of larger than 2 min (as the majority of the analyses do) would produce an even lower occurrence of sequential peaks within the 40 sec interval. It is concluded that the frequency of occurrence of non-independent sequential peaks is much smaller than 10% in this study and, thus, the effects are minor.

Results

Fig. 5 shows the result from one column in Table 5, the t_{pk_g} = 20 min case. The four columns in each plot correspond to the four n_{pk_g} values in Table 5 and each plot presents the results from a different tap. The Cp_{pk_g} from the individual sub-records within a given 30-hr record are plotted as closed circles. The average among all Cp_{pk_g} samples in a column ($\overline{Cp}_{pk\_g}$) is shown as the open circle. The 95% probability range among all Cp_{pk_g} samples in a column is presented as the black cross (denoted as U_{pk_g}) when the number of estimated peaks (n_{peak}) is more than 60 (such as the combination of t_{pk_g} =2 min & n_{pk_g} =30). If n_{peak} is less than 3 (such a case of t_{pk_g} = 30 min & n_{pk_g} =30), simple maximum and minimum values of Cp_{pk_g} are plotted instead of 95% bounds. The empirical value, Cp_{emp}, was calculated using the 30-hr record for the tap and presented along with the +/- 3 standard error (S.E.) range (U_{emp}), which corresponds to 99% confidence interval, as the solid and dashed horizontal gray lines.

Results of all cases in Table 5 are presented in condensed form in Fig. 6. $\overline{Cp}_{pk\_g}$ is the open circle with 95% bounds as indicated by the icons in the legend. Cp_{emp} and its bounds (U_{emp} =Cp_{emp} +/- 3 S.E.) are the horizontal solid and dashed gray lines, respectively.

General observations are first made regarding the magnitude, precision and accuracy of the Cp_{pk_g} estimated from the sub-records. The magnitude of Cp_{pk_g} increases with t_{pk_g} for any given

254 n_{pk_g}, as does the magnitude of Cp_{emp}, observed as the upward trend moving from left to right for
255 each of the four plots in Fig. 6. The precision of Cp_{pk_g} improves with increasing number of
256 observed peaks (n_{pk_g}). This is qualitatively viewed as inversely proportional to the U_{pk_g} range
257 (e.g., black crosses in Fig. 5), observed as the left to right trend in any plot in Fig. 5 and the left to
258 right trend for any given t_{pk_g} in Fig. 6.

259 The mean squared error (*MSE*) quantification of the difference between the individual
260 estimates of Cp_{pk_g} and the empirically evaluated benchmark Cp_{emp} for each tap was calculated
261 using:

262 $$MSE = \frac{1}{n_{peak}} \sum_{i=1}^{n_{peak}} (s_i)^2 \tag{3a}$$

263

where

264 $$s_i = \begin{cases} Cp_{pk\_g,i} - (Cp_{emp,j} + 3 * S.E.), & \left(Cp_{pk\_g,i} > Cp_{emp,j} + 3 * S.E.\right) \\ 0, & \left(Cp_{emp,j} - 3 * S.E. < Cp_{pk\_g,i} < Cp_{emp,j} + 3 * S.E.\right) \\ (Cp_{emp,j} - 3 * S.E.) - Cp_{pk\_g,i}, & \left(Cp_{pk\_g,i} < Cp_{emp,j} - 3 * S.E.\right) \end{cases} \tag{3b}$$

265 and n_{peak} is the number of Cp_{pk_g} samples at a given combination of t_{pk_g} and n_{pk_g} (parenthetical
266 values in Table 5). The results are not presented here (because of space limitations) but *MSE* is
267 generally observed to decrease as n_{pk_g} increases. However, there is no clear monotonic trend
268 between *MSE* and t_{pk_g}.

269 The accuracy of Cp_{pk_g} is quantified by the difference between the $\overline{Cp}_{pk\_g}$ and Cp_{emp}. No clear
270 trend as a function of t_{pk_g} and n_{pk_g} is observed in the error between the open circle and gray solid
271 line in any plots in Fig. 6. Hence, the magnitude and precision of Cp_{pk_g} are influenced by t_{pk_g} and
272 n_{pk_g}, respectively, while the accuracy is not clearly influenced for the range of t_{pk_g} and n_{pk_g} values
273 used in this study.

The accuracy has little meaning without knowledge of the associated precision, as measurement durations for typical applications of the Gumbel estimate of Cp_{pk} provide a single sample rather than multiple samples by which $\overline{Cp}_{pk\_g}$ can be quantified. Thus, it is relevant to offer some quantitative observations regarding the influence of n_{pk_g} on precision. The Cp_{pk_g} precision for different n_{pk_g} varies with taps and t_{pk_g}. A change of n_{pk_g} from 5 to 10 significantly increases the precision of Cp_{pk_g} and reduces the occurrence of Cp_{pk_g} samples that fall outside the U_{emp} range (gray dashed lines in Fig. 6).

These observed trends validate known concepts from extreme value theory. The contribution of this study is to offer a detailed quantification of the uncertainty involved in common practice, where relatively short duration records are used and the opportunity to observe the precision and accuracy (via multiple Cp_{pk_g} and the empirical Cp_{emp}) is not typically available.

This precision quantification provides guidelines for the selection of n_{pk_g} required to achieve acceptable precision. For example, this could be defined as the case where U_{pk_g}, which is the 95% bounds on the estimated Cp_{pk_g}, is contained within U_{emp}, which is the 99% confidence interval associated with Cp_{emp}. In Fig. 6, the n_{pk_g} which achieves $U_{emp} > U_{pk\_g}$ is different depending on t_{pk_g} and tap locations, and it is difficult to find a clear trend in their relationships. When n_{pk_g} needs to be selected for unspecified values of t_{pk_g}, $n_{pk\_g} = 30$ can satisfy the relationship of $U_{emp} > U_{pk\_g}$ for all 4 taps. Although $U_{emp} > U_{pk\_g}$ can still be achieved for many cases in Fig. 6 with $n_{pk\_g} = 15$, it cannot be with $n_{pk\_g} = 10$ for more than half of the cases considered in Fig. 6. With $n_{pk\_g} = 5$, there is no case which satisfies the $U_{emp} > U_{pk\_g}$ relationship regardless of t_{pk_g} and tap location.

The above analysis is expanded to all 493 taps in Fig. 7 wherein the difference between U_{pk_g} and U_{emp}, defined as the following equations, divided by $|Cp_{emp}|$ is presented as a function of $|Cp_{emp}|$ for the combinations of $t_{pk\_g} = 30$ min and all considered n_{pk_g} values in this analysis.

297 $$e_i = \begin{cases} U_{pk\_g,i} - U_{emp,i}, & \left(U_{pk\_g,i} > U_{emp,i}\right) \\ 0, & \left(U_{emp,i} < U_{pk\_g,i} < U_{emp,i}\right) \\ U_{emp,i} - U_{pk\_g,i}, & \left(U_{pk\_g,i} < U_{emp,i}\right) \end{cases} \quad (4)$$

298 where i denotes the tap number.

299 Recall that $U_{\text{pk\_g}}$ is the 95% probability range among individual $Cp_{\text{pk\_g}}$ at a given tap. The
300 uncertainty range U_{emp} in Figs. 5 and 6 is also a function of the individual tap, hence, e can be
301 calculated for each tap and presented as a percentage.

302 With $n_{\text{pk\_g}} \geq 10$, $|e / Cp_{\text{emp}}|$ for most of the taps are within 20% range except for those with low
303 magnitude peaks and with low kurtosis values. Large $|GCp|$ values defined for C&C in ASCE7-10
304 are around 3 (noting that the code values are area averages). Using the conversion method of St.
305 Pierre et al. (2005), this corresponds to values around 3.6 for the Cp values utilized in the current
306 analysis, which are referenced to mean-hourly wind speed measured at 10m height in suburban
307 terrain. Considering the differences of the target peak fractile levels, $|Cp_{\text{emp}}| \approx 4$ may be the
308 magnitude level which needs to be focused on in the current study. For the large majority of taps
309 with the peaks with this magnitude level ($|Cp_{\text{emp}}| > 4$), $|e / Cp_{\text{emp}}|$ is within 10% range with $n_{\text{pk\_g}} \geq$
310 15 with no significant improvement obtained by increasing $n_{\text{pk\_g}}$ to values greater than 15 except
311 for peaks with low magnitude and low kurtosis values. Fig. 7 also includes a mean and standard
312 deviation of mean squared error (MSE_{mean}, MSE_{STD}, respectively) quantification using:

313 $$MSE_{mean} = \frac{1}{n_{tap}} \sum_{j=1}^{n_{tap}} MSE_j \qquad MSE_{STD} = \sqrt{\frac{1}{n_{tap}} \sum_{j=1}^{n_{tap}} \left(MSE_{mean} - MSE_j\right)^2} \quad (5)$$

314 where MSE_{j} is the MSE defined in Eq. (3a) at tap j, and n_{tap} is the number of taps (493).

315 The statistics of MSE are dramatically reduced by increasing $n_{\text{pk\_g}}$ and considering the
316 magnitude of $|Cp_{\text{emp}}|$, the error defined in Eq. (3b) is less than 1% of $|Cp_{\text{emp}}|$ on average for $n_{\text{pk\_g}}$
317 $\geq$ 10, meaning that most of the estimated peaks are within U_{emp} (=Cp_{emp} +/- 3 S.E.) regardless of

tap location. The effects of t_{pk_g} on the relationship between U_{emp} and U_{pk_g} are not clearly seen in Fig. 6. However by expanding the analysis to 493 taps in Fig. 7, it was found that $U_{emp} > U_{pk\_g}$ can be achieved with less n_{pk_g} for smaller t_{pk_g}, hence, the observations made above are applicable to $t_{pk\_g} < 30$ min as well.

For a fixed time frame within a wind tunnel experiment (t_{total}), reducing t_{pk_g} provides a means to increase n_{pk_g} and, thus, the precision of the resulting Cp_{pk_g}. However, the magnitude of the estimated Cp_{pk_g} is only significant within the frame of reference of the duration in which it is quantified (t_{pk_g}). Results from experiments utilizing different t_{pk_g} cannot be directly compared absent a common frame of reference. It will be confirmed in the next section that Cp_{pk_g} based on a given t_{pk_g} and n_{pk_g} can be converted to an equivalent Cp_{pk_g} for the same n_{pk_g} and another (larger) t_{pk_g}. This conversion comes at the cost of some loss of precision and accuracy.

Evaluation of t_{pk_g} conversions

The selection of t_{pk_g} in practice is driven largely by the need to provide a sufficiently large n_{pk_g} within a fixed total sampling time (t_{total}). A relatively short duration of t_{pk_g} is typically used due to the preference for wind tunnel testing times of 15-60 min, particularly for the larger model scales used for low-rise buildings. A conversion for Cp_{pk_g} among various t_{pk_g} was evaluated by Cook and Mayne (1979), and allows the estimate of Cp_{pk} using limited data (large n_{pk_g}, small t_{pk_g}), followed by a conversion of Cp_{pk_g} from a smaller t_{pk_g} to that of a larger t_{pk_g} that can serve as a common frame of reference, e.g., for use in design. Cook and Mayne (1979) presented a conversion for Gumbel parameters (α, U):

$$\alpha_T = \alpha_t \tag{6}$$

$$U_T = U_t + \ln(T/t)/\alpha_t \tag{7}$$

where α_T and U_T are Gumbel parameters for $t_{pk\_g} = T$, and α_t and U_t are those for $t_{pk\_g} = t$ (where $T > t$). The Gumbel parameters are fitted to the observed peaks using a t_{pk_g} of t minutes, and then converted to parameters for an equivalent $t_{pk\_g} = T$-min Gumbel distribution. This allows conversion between different t_{pk_g}, T and t under the condition that both T and t are long enough to ensure the statistical independence of peaks (Cook 1985), and ideally lie in the spectral gap range (i.e., 10-min to 60 min, Van de Hoven 1956; Cook 1982; 1985) so that peaks are due only to turbulence effects and not to changes in the storm or other large-scale environmental factors.

The efficacy of this conversion (Eqs. (6) & (7)) was investigated in Cook (1982; 1985). The n_{pk_g} is unknown (not reported), and durations of T=60 min and t=10 and 1 min were examined. It was found that the agreement between the measurements for the T=60min and the data predicted from t=10min is very good, while the use of t=1 min resulted in overestimates of 10-20%. Using the current dataset, Eqs. (6) & (7) are investigated as a function of n_{pk_g}. The precision of the conversion from t_{pk_g} values smaller than 10 min but larger than 1 min is also investigated. These two issues have not been examined in previous studies, and are critical to the objective of selecting n_{pk_g} and t_{pk_g} with known uncertainty for a given fixed test time t_{total}.

60-min is commonly used in wind tunnel studies for high-rise buildings as the duration of the measurements, consistent with the averaging time of the wind velocities (the averaging time for a basic wind velocity and the evaluation time for Cp_{pk} should be the same; Cook and Mayne 1979; Cook 1982). In hurricanes, wind speeds are rarely stationary for such a long duration, with 10-15 min being more typical. It is important to consider that the peak pressures being assessed are directly related to turbulence effects and that the physical processes are stationary so that meteorological effects do not play a role. T = 60 min is at the upper bound of reasonable duration to be associated with peak wind speeds in a storm and was selected in the current study.

A set of Gumbel parameters (U_{60min}, α_{60min}) was calculated for all 493 taps using n_{pk_g} = 30 & t_{pk_g} = 60 min and the 80% fractile Cp_{pk_g} samples were estimated using these Gumbel parameters (denoted as '$Cp_{pk\_g\_60}$'). Another set of Gumbel parameters (U_t, α_t) was calculated for each tap using t_{pk_g} =2, 5 and 10 min and n_{pk_g} =10, 15 and 30 (t_{total} = 10 – 600 min sub-records) and converted to 60-min equivalents using Eqs. (6) & (7). Peaks calculated in this way are denoted as '$Cp_{pk\_g\_t}$' where t can be 2, 5 and 10. For each tap, the ratio between $Cp_{pk\_g\_60}$ and $Cp_{pk\_g\_t}$ are calculated as a range using the maximum and minimum estimated peaks of $Cp_{pk\_g\_t}$, and are shown in Fig. 8 as a function of $|Cp_{pk\_g\_60}|$. The broken horizontal lines in the figures indicate +/-10% and +/- 20% ranges of $|Cp_{pk\_g\_t}|/|Cp_{pk\_g\_60}|$. The reduced number of peaks (n_{pk_g}) and its sampling duration (t_{pk_g}) associated with shorter records results in a loss of precision. In addition, taps with large kurtosis values have less variation in $|Cp_{pk\_g\_t}|/|Cp_{pk\_g\_60}|$. Focusing on peak coefficients with magnitudes larger than 4, combinations of n_{pk_g} =15 and $t_{pk\_g} \geq$ 10 min, n_{pk_g} =30 and $t_{pk\_g} \geq$ 5 min can estimate $Cp_{pk\_g\_t}$ which are within 20% of difference from $Cp_{pk\_g\_60}$.

In light of these results, the analysis used to produce Figs. 5 and 6 was appended with an additional step. The individual estimation of Cp_{pk_g} (80% fractile) for various t_{pk_g} and n_{pk_g} listed in Table 5 were converted to an equivalent t_{pk_g} =60-min value using Eqs. (6) & (7). Cp_{emp} was then calculated from the empirical CDF using t_{pk_g} =60 min & n_{pk_g} =30. The results are shown in Fig. 9.

We seek to minimize the wind tunnel test time, t_{total}, required to achieve acceptable precision, in which the 95% bounds of the Cp_{pk_g} (U_{pk_g}) are contained within U_{emp} (= Cp_{emp} +/- 3S.E.), including the influence of the conversion (Eqs. (6) & (7)) for different t_{pk_g} & n_{pk_g} combinations.

With the exception of tap 2, the use of t_{pk_g} = 2, 5 min produces large uncertainty regardless of n_{pk_g}. By increasing t_{pk_g} to 10, 20 and 30 min, the $U_{emp} > U_{pk\_g}$ relationship can be achieved by

386 using the number of n_{pk_g} of 30, 15 and 10, respectively, with a few exceptions. Note that the
387 combination of t_{pk_g} and n_{pk_g} which satisfies the $U_{emp} > U_{pk\_g}$ relationship requires longer t_{total} than
388 that selected based on the applicability of Eqs. (6) & (7) in Fig. 8.

389 The above examination was expanded to all 493 taps and the results are presented in Fig. 10
390 with n_{pk_g} =10, 15, 30 and t_{pk_g} =5, 10, 20 min. The variation of $|e/Cp_{emp}|$ changes with both n_{pk_g}
391 and t_{pk_g}. As expected, large n_{pk_g} values, with a smaller extrapolation of t_{pk_g} leads to more accurate
392 results. The question to be answered is what is sufficient. Considering the other uncertainties in
393 developing design wind loads, a 95% probability range covering approximately ±10% for the large
394 magnitude coefficients should be acceptable in practice, given that the overall expected coefficient
395 of variation for wind loads on structures is about 35% (Ellingwood 1999). At this level, the random
396 variations of peak pressures would not significantly alter the reliability of the final answer.
397 Therefore, viewing Fig. 10 with this acceptable range in mind, and focussing on the coefficients
398 with magnitudes of about 4 and higher, t_{pk_g} = 5 or 10 min can be utilized with n_{pk_g} =30 and t_{pk_g}
399 =20 min with $n_{pk_g} \geq$15. The results are not presented but t_{pk_g} =2 min and n_{pk_g} =5 cannot be
400 selected regardless of n_{pk_g} and t_{pk_g}, respectively. Thus, for T = 60 min, the minimum wind tunnel
401 test duration is about 150 min using t_{pk_g} = 5 min with n_{pk_g} = 30. Thus, the extrapolation of t_{pk_g}
402 by about an order of magnitude using n_{pk_g} = 30 leads to sufficiently accurate results. This implies,
403 for example, that for T = 10 min, one could use t_{pk_g} = 1 min with n_{pk_g} = 30 for a total sampling
404 duration of about 30 min.

405 **ISO 4354**

406 In the peak estimation method in ISO 4354 (2009), which was introduced at the beginning of the
407 current study, the mean and the standard deviation of the observed peaks are translation and
408 dilation parameters in the estimation of Cp_{pk}. The ISO 4354 Annex D equations D.1 and D.3

409 provide an estimate of the 80% fractile Cp_{pk} for a reference period of 1 hr. These estimates are
410 included in Fig. 9 as the two right most columns in each plot. $U_{pk\_g\_ISO60}$, which is the same as
411 U_{pk_g} but calculated from the estimated Cp_{pk} using ISO 4354 equation D.1, are less than U_{emp} for
412 most of the taps and $n_{pk\_g} > 5$, but requires the wind tunnel testing time of at least 5 hr. The ISO
413 estimates based on t_{pk_g} = 10 min are very similar to those of the Gumbel fitting approach for t_{pk_g}
414 =10 min. That is, the Gumbel fitting approach and the method in ISO 4354 (2009) are almost
415 identical with regard to the uncertainty associated with a common t_{pk_g}, and no obvious advantage
416 to using the ISO approach was identified.

417 To validate this conclusion, the comparison between the Gumbel fitting and ISO approaches
418 was expanded to all 493 taps for the combination of t_{pk_g} =10 min & n_{pk_g} =30 (t_{total} = 300 min),
419 shown in Figs. 11(a) and (b), respectively. The statistics of mean square error (*MSE*) between
420 Cp_{emp} and estimated peaks were also calculated using Eqs. (3) and (4) with n_{tap} =493 and n_{peak} =6.
421 The results from the two methods are visually very similar with the Gumbel fitting approach
422 showing slightly lower *MSE* values. Overall, a clear advantage between the two methods was not
423 identified since both utilize the same observed peaks and have similar results and uncertainty for
424 a common t_{pk_g}.

425 **Effects of area averaging**

426 Thus far, the analyses have focused on local *Cp* time histories measured at single taps. The
427 previous section applied a metric of $U_{pk\_g} < U_{emp}$ (=Cp_{emp} +/- 3 S.E.) to suggest that t_{pk_g} =5 min
428 & n_{pk_g} =30 (t_{total} = 150 min) results in an acceptable precision in the estimation of 80% fractile
429 peak with a 1-hr reference duration. This was the case using both the Gumbel-fitting approach to
430 observed peaks with the conversion to 60-min equivalent Cp_{pk_g} and the application of the ISO
431 4354 method.

Aggregate loads over larger areas are typically of significant concern in determining design loads for both the main wind force resisting system and components and cladding. It is well known that the magnitude of the peak is reduced when area averaging is considered (e.g., Kopp et al., 2005). It is also known that the probability distribution of the area-averaged pressure will differ from those of its individual components when the area becomes larger (e.g., Stathopoulos 1979). This section will consider whether the n_{pk_g} and t_{pk_g} necessary to achieve a desired accuracy and precision of Cp_{pk_g} are altered when area-averaged pressures are analyzed.

A series of 30-hr time histories were constructed via area averaging of multiple adjacent taps, as was done in Gavanski and Uematsu (2014). It was not possible to conduct a tributary area analysis for tap 3 due to its location on the roof. The size and the number of larger areas vary with the tap. Following the analysis of single tap *Cp* time series, Cp_{pk_g} values (80% fractile) were estimated from the area-averaged time histories for various t_{pk_g} and n_{pk_g}, and then converted to an equivalent t_{pk_g} =60-min value. Cp_{emp} was then calculated from the empirical CDF of each of the area averaged time histories using t_{pk_g} =60 min & n_{pk_g} =30.

Fig. 12 presents area-averaged results in a format similar to Fig. 9 for n_{pk_g} =10, 15 and 30. The assigned n_{pk_g} is constant in a given figure (3 figures per tap). The columns in each plot correspond to the area used for averaging and the number of taps employed for the calculation of area-averaged *Cp* time series. The cases where the smallest (base) tributary area was considered utilized *Cp* time series at only one tap, therefore the results are the same as in Fig. 9.

As expected, the magnitude of Cp_{pk_g} is reduced as area increases, to a degree substantially dependent on location. Observing the relationship between Cp_{emp} and U_{pk_g}, there seem to be more cases where U_{emp} (=Cp_{emp} +/- 3 S.E.) begins to contain U_{pk_g} as area increases for large n_{pk_g} regardless of tap location (Fig. 12(c), (f), and (i)). For example with n_{pk_g} =30, while it is necessary

to have t_{total} of 150 min (t_{pk_g} = 5 min) for single tap *Cp* time series in order to have a relationship of $U_{pk\_g} < U_{emp}$ at taps 1, 2 and 4, t_{total} can be reduced to 60 min (t_{pk_g} = 2 min) for area-averaged *Cp* time series. However, for small n_{pk_g}, the relationship of U_{pk_g} and U_{emp} does not necessary improve and in some cases becomes worse as area increases.

CONCLUSIONS

The purpose of this study is to highlight the strong influence of duration and peak sampling frequency on uncertainty. While the sensitivity of uncertainty is undoubtedly a function of estimation method, the duration vs. precision trade-off issue is universal. The wind tunnel practitioner that employs a different estimation method and peak definition may not be able to utilize our specific quantifications, but can benefit from the exposure of the issue and our simple uncertainty quantification scheme rather than the nominal results.

The accuracy and precision of peak pressure coefficient estimation procedures were investigated using wind-tunnel time-series data obtained on the roof of a low-rise building. In particular, the uncertainties due to the use of short duration records (which are often used in practice) are investigated in order to identify the combination of the duration in which a single peak is observed (t_{pk_g}) and number of observed peaks (n_{pk_g}) necessary to achieve various levels of precision that minimizes the total sampling duration within acceptable error bounds. For any sampling time, t_{pk_g}, 30 observed peaks (i.e., n_{pk_g} = 30) were required in order that the difference between true (Cp_{emp}) and estimated peaks (Cp_{pk_g}) had a 95% probability of being within about ±10% of each other (except for taps with relatively small magnitude peak values). However, if only the larger magnitude suctions are of primary concern, using n_{pk_g} = 15 would yield a similar precision. Thus, for many design scenarios, if no extrapolation to other sampling times are required, the use of n_{pk_g} = 15 is likely to be sufficient.

When particular sampling times are required, the combination of both t_{pk_g} and n_{pk_g} need to be investigated. In the current work, it was assumed that the desired sampling duration for the peak, T, is 60-min, consistent with earlier studies and design standards. The conversion of Gumbel parameters, derived from peaks observed from a series of subsets with duration, t_{pk_g}, less than 60 min to those associated with $t_{pk\_g} = T = 60$ min, was applied to the peak estimation procedure. Precision was evaluated in terms of both t_{pk_g} and n_{pk_g}. Errors and uncertainty increase when the extrapolation procedure is used such that extrapolating from $t_{pk\_g} = 2$ min to 60 min (i.e., a factor of 30) with $n_{pk\_g} = 30$ leads to differences between the true and estimated peaks with a 95% probability of being within about ±20% of each other for the majority, though certainly not all, of the taps. However, for the extrapolation from $t_{pk\_g} = 10$ min to 60 min, the majority of the larger magnitude peaks are within ±15% when $n_{pk\_g} = 30$ and within ±20% when $n_{pk\_g} = 15$. Considering the other uncertainties in developing design wind loads, a 95% probability range covering approximately ±10% for larger magnitude peaks should be acceptable in practice, given that the overall expected coefficient of variation for wind loads on structures is about 35% (Ellingwood 1999). Thus, if T is required to be 60-min, then the total minimum sampling time duration is about $t_{total} = 150$ min (with $t_{pk\_g} = 5$ min and $n_{pk\_g} = 30$). If T is required to be only 10-min, then, holding the same extrapolation ratio, the total minimum sampling time duration is about $t_{total} = 30$ min (with $t_{pk\_g} = 1$ min and $n_{pk\_g} = 30$). The analysis of area-averaged coefficients leads to a similar conclusion but with slight improvement on the estimation accuracy and precision for large n_{pk_g}. Thus, current wind tunnel studies that acquire data for about 30 min in equivalent full-scale, will have sufficient accuracy for 10 min statistics if 30, 1-min peaks are used.

Finally, the peak estimation procedure in ISO 4354 was compared with the Gumbel-fitting approach using equivalent input (common t_{pk_g} and n_{pk_g}). No advantage was identified between methods with regard to the resultant uncertainties in the estimated Cp_{pk_g}.

ACKNOWLEDGEMENTS

The experimental data was obtained with support from NSF CMMI-0928563.

NOTATION

The following symbols are used in this paper:

Cp= Pressure coefficient;

Cp_{emp}= Peak pressure coefficient calculated from empirical cumulative distribution function of F_{emp} with n_{pk_g} =60 and fractile level (F_{pk_frac}) of 80% for a certain t_{pk_g};

Cp_{pk}= Peak pressure coefficient;

Cp_{pk_g}= Peak pressure coefficient estimated from Gumbel modeled cumulative distribution function (F_g);

$Cp_{pk\_g\_60}$= Estimated peak pressure coefficient with peak evaluation time (t_{pk_g}) of 60 min (full-scale) without the use of Cook-Mayne conversion;

$Cp_{pk\_g\_t}$=Estimated peak pressure coefficient calculated using peaks whose peak evaluation time (t_{pk_g}) of t min (full-scale) and converted to 60-min equivalent using Cook-Mayne conversion;

$\overline{Cp}_{pk\_g}$= Average of Cp_{pk_g};

e= Difference between U_{pk_g} and U_{emp};

F_{emp}= Empirical cumulative distribution function;

F_g= Gumbel modeled cumulative distribution function;

F_{pk_frac}= Peak fractile level set for the estimated peak pressure coefficient;

MSE= Mean square error between the individual estimated peaks (Cp_{pk_g}) and empirically estimated peak (Cp_{emp});

n_{pk_g}= Number of observed peak from Cp times series used for the calcualtion of Cp_{pk_g};

n_{peak}= Number of Cp_{pk_gum} estimated from 30-hr (full-scale) Cp time series for a certain combination of t_{pk_g} and n_{pk_g};

t_{pk_g}= Peak evaluation time;

t_{total}= Total testing time required to estimate Cp_{pk_g}, which is ($t_{pk\_g} \times n_{pk\_g}$);

U_{emp} =Cp_{emp} +/- 3 standard error (S.E.) range;

U_{pk_g}=95% probability range of all Cp_{pk_g} estimated for a certain combination of t_{pk_g} and n_{pk_g}.

REFERENCES

ASCE (American Society of Civil Engineers). (2010). "Minimum design loads for buildings and other structures." ASCE7-10, Reston, VA, USA.

AIJ (Architectural Institute of Japan). (2004). "Architectural Institute of Japan, Recommendations for loads on buildings." AIJ-RLB-2004, Tokyo, Japan.

AS/NZS (Australia New Zealand Standard), (2002). "Structural design actions, Part 2: Wind actions." AS/NZS-1170.2, Standards Australia, Sydney, NSW, Australia.

Australian wind engineering society. (1994). "Quality assurance manual - Cladding pressure and environmental wind studies." AWES-QAM-1-1994.

BS EN1991-1-4. (2005). "Eurocode 1: Actions on Structures. Part 1-4: General Actions. Wind Actions."

Cook, N. J., Mayne, J. R. (1979). "A novel working approach to the assessment of wind loads for equivalent static design." J. Wind. Eng. Ind. Aerodyn., 4(2), 149-164.

Cook, N. J. (1982). "Calibration of the quasi-static and peak-factor approaches to the assessment of wind loads against the method of Cook and Mayne." J. Wind. Eng. Ind. Aerodyn., 10(3), 315-341.

Cook, N. J. (1985). "The designer's guide to wind loading of building structures." Building Research Establishment, Butterworths, London.

Dalgliesh, W.A., Templin, J.T., 1980. Comparisons of wind tunnel and full-scale building surface pressures with emphasis on peaks. Wind Engineering, Proceedings 5th Int. Conf., J.E. Cermak, ed., Pergamon Press.

Davenport, A.G., 1964. Note on the distribution of the largest value of a random function with application to gust loading. Proceedings Inst. Of Civil Engineers, 28, pp. 187-196.

Ellingwood, B.R. (1999). “Requirements in building codes in Canada, Mexico, and the United States.” Eng. J., 36(2), 67-80.

Gavanski, E., Uematsu, Y. (2014). “Local wind pressures acting on walls of low-rise buildings and comparisons to the Japanese and US wind loading provisions.” J. Wind. Eng. Ind. Aerodyn., 132, 77-91.

Geurts, C.P.W., Kopp, G.A., Morrison, M.J. (2013). “A review of the wind loading zones for flat roofs in code provisions.” Proc. of the 6th European and African Conference on Wind Engineering, Cambridge, July 2013, 1-6.

Geurts, C.P.W., Zimmerli, B., Hansen, S.O., Van Staalduinen, P., Sedlacek, G., Hortmanns, M., Spehl, P., and Blackmore, P. (2001). “Transparency of pressure and force coefficients.” Proc. of the 3rd European and African Conference on Wind Engineering, 165-172.

Harris, R.I. (2001). “The accuracy of design values predicted from extreme value analysis.” J. Wind. Eng. Ind. Aerodyn., 89(2), 153-164.

Harris, R.I. (2009). “XIMIS, a penultimate extreme value method suitable for all types of wind climate.” J. Wind. Eng. Ind. Aerodyn., 97(5-6), 271-286.

Holmes, J. D., Moriarty, W. W. (1999). “Application of the generalized Pareto distribution to extreme value analysis in wind engineering.” J. Wind. Eng. Ind. Aerodyn., 83(1-3), 1-10.

Holmes, J. D., Cochran, L. S. (2003). “Probability distributions of extreme pressure coefficients.” J. Wind. Eng. Ind. Aerodyn., 91(7), 893-901.

Hong, H.P., Li, S.H. and Mara, T.G. (2013). “Performance of the generalized least-squares method for the Gumbel distribution and its application to annual maximum wind speeds.” Wind. Eng. Ind. Aerodyn., 119(7), 121-132.

ISO (International Organization for Standardization). (2009). “Wind actions on structures. International Organization for Standardization.” ISO 4354:2009, Switzerland.

Kasperski, M., 1997. Specification and codification of design wind loads. Rep., Fakultat fur Bauingenieurwesen, Ruhr-Universitat, Bochum, Germany.

Kasperski, M. (2003). “Specification of the design wind load based on wind tunnel experiments.” J. Wind. Eng. Ind. Aerodyn., 91(4), 527-541.

Kasperski, M. (2009). “Specification of the design wind load – A critical review of code concepts.” J. Wind. Eng. Ind. Aerodyn., 97(7-8), 335-357.

Kopp, G.A., Gavanski, E. (2010). “Wind tunnel pressure measurements on two FCMP houses in Florida.” Res. Rep. BLWT-5-2010, The Boundary Layer Wind Tunnel Laboratory, Univ. of Western Ontario, London, ON, Canada.

Kopp, G. A., Surry, D., Mans, C. (2005). “Wind effects of parapets on low buildings: Part 1. Basic aerodynamics and local loads.” J. Wind. Eng. Ind. Aerodyn., 93(11), 817-841.

Krishnan, V. (2006). “Probability and random processes.” Wiley, New Jersey, USA.

Lieblein, J. (1974). “Efficient methods of extreme-value methodology.” Rep. No. NBSIR 74-602, National Bureau of Standards, Washington, DC.

Liu, Z., Prevatt, D.O., Aponte-Bermudez, L.D., Gurley, K.R., Reinhold, T.A., Akins, R.E. (2009). “Field measurement and wind tunnel simulation of hurricane wind loads on a single family dwelling.” Eng. Struct., 31(10), 2265-2274.

NBCC (National Building Code of Canada). (2010). “National Building Code of Canada 2010.” Institute for Research in Construction, National Research Council of Canada, Ottawa, Ont., Canada.

Peng, X., Yang, L, Gavanski, E., Gurley, K., and Prevatt, D. (2014). "A comparison of methods to estimate peak wind loads on buildings." J. Wind. Eng. Ind. Aerodyn., 126, 11-23.

Peterka, J. A., 1983. Selection of local peak pressure coefficients for wind tunnel studies of buildings. J. Wind. Eng. Ind. Aerodyn. 13(1-3), pp. 477-488.

Peterka, J.A., and Cermak. (1975). "Wind pressure on buildings-probability densities." J. Struct. Div., 101(6), 1255-1267.

Quan, Y., Gu M., Tamura Y., and Chen B. (2009). "An extreme-value estimating method of non-Gaussian wind pressure." The 7th Asia-Pacific conference on wind engineering, November 8-12, 2009, Taipei, Taiwan.

Sadek, F. and Simiu, E., 2002. Peak non-Gaussian wind effects for databse-assisted low-rise building design. J. Eng. Mech., 128(5), 530-539.

Simiu, E. and Heckert, N.A. (1996). "Extreme wind distribution tails: A "peaks over threshold" approach." J. Struct. Eng., 122(5), 539-548.

Sockel, H., 1980. Local pressure fluctuations. Wind Engineering, Proceedings 5th Int. Conf., J.E. Cermak, ed., Pergamon Press.

Stathopoulos, T. (1979). "Turbulent wind action on low rise buildings." PhD. Thesis, University of Western Ontario, London, Ontario, Canada.

Stathopoulos, T., Wang, K., and Wu, H. (2001). "Wind pressure provisions for gable roofs of intermediate roof slope." Wind. Struct., 4(2), 119-130.

St. Pierre, L. M., Kopp, G. A., Surry, D. and Ho, T. C. E. (2005). "The UWO contribution to the NIST aerodynamic database for wind loads on low buildings: Part 2. Comparison of data with wind load provisions." J. Wind. Eng. Ind. Aerodyn., 93(1), 31-59.

The Building Center of Japan. (2008). “Guide book on wind tunnel testing of building structures for practitioners (translated).” ISBN978-4-88910-148-5.

Van de Hoven, I. (1956). “Power spectrum of horizontal wind speed in the frequency range from 0.0007 to 900 cycles per hour.” J. Meteorology, 14, 160-164.

Wilcox, R. (2012). “Introduction to robust estimation and hypothesis testing.” Elsevier.

FIGURE CAPTIONS

Fig. 1. Statistics of parameters for Gumbel fitting method utilized in previous studies: (a) peak sampling duration in full-scale, (b) peak sampling duration in model-scale, (c) number of peaks observed, (d) peak fractile level.

Fig. 2. Plan view of the building model, with the tap locations 1 – 4 indicated. The arrow indicates the wind direction used in the analysis.

Fig. 3. Skewness and kurtosis pair of *Cp* data measured at 493 taps.

Fig. 4. Observed values of Cp_{pk_g} for t_{pk_g}=18 min & n_{pk_g}=100, as well as fits to the Gumbel distribution using several methods: (a) Tap 1, (b) Tap 2, (c) Tap3, and (d) Tap 4.

Fig. 5. Plots of Cp_{pk_g} for all n_{pk_g} with t_{pk_g} =20 min, from single tap *Cp* time histories at the 4 selected taps in Fig. 2: (a) Tap 1, (b) Tap 2, (c) Tap3, and (d) Tap 4. Values shown are the estimated values of Cp_{pk_g} (●) and its mean, $\overline{Cp}_{pk\_g}$ (○), and 95% probability range, U_{pk_g} (+). Also included are the peak values from the empirical distribution, Cp_{emp} (solid gray line), and U_{emp} range (dashed gray line).

Fig. 6. Plots of Cp_{pk_g} for all n_{pk_g} and t_{pk_g} from single tap *Cp* time histories at the 4 selected taps in Fig. 2: (a) Tap 1, (b) Tap 2, (c) Tap3, and (d) Tap 4. Values shown are the mean of the estimated peak, $\overline{Cp}_{pk\_g}$ (○), and 95% probability range, U_{pk_g} (*, ●, +, ■). Also included are the peak values from the empirical distribution, Cp_{emp} (solid gray line), and U_{emp} range (dashed gray line).

Fig. 7. Plots of peak values from the empirical distribution, Cp_{emp} (horizontal axis) and the difference between U_{pk_g} and U_{emp} divided by Cp_{emp} (vertical axis) for all 493 taps for t_{pk_g} =30 min: (b) n_{pk_g} =10, (c) n_{pk_g} =15.

Fig. 8. Cp_{pk_g} values for t_{pk_g} = 60 min ("$Cp_{pk\_g\_60}$"), those for t_{pk_g} = 2, 5, and 10 min converted to 60 min using Eqs. (6) & (7) ("$Cp_{pk\_g\_2}$, $Cp_{pk\_g\_5}$, $Cp_{pk\_g\_10}$"), as well as the +/-10 and 20% ranges of estimated values (horizontal dashed gray lines).

Fig. 9. Plots of Cp_{pk_g} for all n_{pk_g} and t_{pk_g}, from single tap Cp time histories at the 4 selected taps (Fig. 2) with conversion to t_{pk_g} =60 min using Eqs. (6) & (7): (a) Tap 1, (b) Tap 2, (c) Tap3, and (d) Tap 4. Values shown are the mean of the estimated peak, $\overline{Cp}_{pk\_g}$ (○), and 95% probability range, U_{pk_g} (*, ●, +, ■). Also included are the peak values from the empirical distribution, Cp_{emp} (solid gray line), U_{emp} range (dashed gray line), and 95% probability range of ISO peaks calculated with t_{pk_g} =10 min and 60 min for various n_{pk_g}, $U_{pk\_g\_ISO}$.

Fig. 10. Plots of peak values from the empirical distribution, Cp_{emp} (horizontal axis) and the difference between U_{pk_g} and U_{emp}, e, divided by Cp_{emp} (vertical axis) for all 493 taps.

Fig. 11. Plots of peak values from the empirical distribution, Cp_{emp} (horizontal axis) and (a) the difference between U_{pk_g} and U_{emp} divided by Cp_{emp} (vertical axis) where U_{pk_g} calculated using Gumbel fitting approach for t_{pk_g} = 10 min & n_{pk_g} =30 converted to 60 min using Eqs. (6) & (7), and (b) the difference between $U_{pk\_g\_ISO}$ and U_{emp} divided by Cp_{emp} (vertical axis) where $U_{pk\_g\_ISO}$ calculated for t_{pk_g} = 10 min & n_{pk_g} =30 for all 493 taps in Fig. 2.

Fig. 12. Plots of Cp_{pk_g} for n_{pk_g} =10, 15, 30 and all t_{pk_g} from area-averaged Cp histories at the 3 selected taps with conversion to t_{pk_g} =60 min using Eqs. (6) & (7).Values shown are the mean of the estimated peak, $\overline{Cp}_{pk\_g}$ (○), and 95% probability range, U_{pk_g} (*, ●, +, ■, ×). Also included are the peak values from the empirical distribution, Cp_{emp} (solid gray line) and U_{emp} range (dashed gray line).

TABLES

Table 1: Statistics of peak estimation method preference in previous studies sorted by decadal era

Method	1970s	1980s	1990s	2000s	2010s	total
Simple worst	2	8	12	5	16	43
Ensemble-average	1	1	12	12	16	42
Gumbel fitting	0	0	4	9	13	26
Cook-Mayne method	0	1	1	2	16	20
Translation method	0	0	0	2	6	8
Peak factor method	0	0	0	1	4	5
Not mentioned	0	1	3	3	3	10
Other	0	0	1	2	2	5
total	3	11	33	36	76	159

Table 2: Statistics of peak estimation method preference in previous studies sorted by region

Method	N & S America	Europe	Asia	Oceania	total
Simple worst	22	5	12	4	43
Ensemble-average	18	2	16	6	42
Gumbel fitting	16	5	2	3	26
Cook-Mayne method	0	9	11	0	20
Translation method	6	0	2	0	8
Peak factor method	0	2	3	0	5
Not mentioned	2	1	7	0	5
Other	3	0	1	1	10
total	67	24	54	14	159

Table 3: Peak estimation method described in national codes

Authority	Design code	Explicit explanation of peak estimation in code	Possible method utilized for calculating design value in codes	Detail of calculation method
Australia/ New Zealand	AS/NZ Standard	No	Ensemble-average (Quality assurance manual cladding pressure and environmental wind studies, 1994)	n_{pk_g} =6 t_{pk_g} =10 min – 3 hrs (FS)
Canada	NBCC	No	Single measured peak based on Stathopoulos (1979)	N/A
Europe	BS-EN 1991-1-4	No	A single measured peak based on Stathopoulos (1979); see Geurts et al. (2013)	N/A
ISO	ISO 4354	80% fractile value of the extreme aerodynamic coefficient assuming the peaks follow a Gumbel distribution	N/A	n_{pk_g}: n/a t_{pk_g} =10 – 60 min (FS) F_{pk_frac}= 80%
Japan	Building Standard of Japan, AIJ Recommendations	No	Ensemble-average of several peaks based on Guide book on wind tunnel testing of building structures for practitioners (2008)	n_{pk_g} =6 - 15 t_{pk_g}=10 min (FS)
US	ASCE7	P_{max} in $Cp_{max}=P_{max}/q_{ref}$ is "maximum instantaneous pressure measured over the sampling period" in ASCE/SEI49-12.	Ensemble-average of several peaks with some adjustment for intermediate roof slope based on Stathopoulos et al. (2001)	n_{pk_g}=6 t_{pk_g}=10 min (FS)

Table 4: Statistics of *Cp* at the four taps identified in Fig. 2

Statistics	Tap1	Tap2	Tap3	Tap4
Mean	-1.69	-1.36	-0.33	-0.29
Max	0.34	0.58	1.47	1.56
Min	-12.9	-9.98	-9.26	-6.79
S.D.	0.90	0.66	0.33	0.31
COV	-0.53	-0.48	-1.00	-1.09
Skewness	-1.34	-1.18	-2.64	-2.26
Kurtosis	5.69	5.41	21.04	15.47

Table 5: Combinations of parameters used in the statistical analysis

Cell content: t_{total} (minutes) (n_{peak})		t_{pk_g} (minutes)				
		2	5	10	20	30
n_{pk_g}	5	10 (180)	25 (72)	50 (36)	100 (18)	150 (12)
	10	20 (90)	50 (36)	100 (18)	200 (9)	300 (6)
	15	30 (60)	75 (24)	150 (12)	300 (6)	450 (4)
	30	60 (30)	150 (12)	300 (6)	600 (3)	900 (2)

Table 6: Nomenclature

Definitions	
Cp	Pressure coefficient time series
Cp_{pk}	Peak pressure coefficient
Cp_{pk_g}	Peak pressure coefficient estimated from Gumbel modeled cumulative distribution function (F_g)
Cp_{emp}	Peak pressure coefficient calculated from empirical cumulative distribution function of F_{emp} with n_{pk_g} =60 and fractile level of 80% for a certain t_{pk_g}
$Cp_{pk\_g\_60}$	Estimated peak pressure coefficient with peak evaluation time (t_{pk_g}) of 60 min (full-scale) without the use of Cook-Mayne conversion
$Cp_{pk\_g\_t}$	Estimated peak pressure coefficient calculated using peaks whose peak evaluation time (t_{pk_g}) of t min (full-scale) and converted to 60-min equivalent using Cook-Mayne conversion
$\overline{Cp}_{pk\_g}$	Average of Cp_{pk_g}
t_{pk_g}	Peak evaluation time
n_{pk_g}	Number of peak from Cp times series used for the calcualtion of Cp_{pk_g}
n_{peak}	The number of Cp_{pk_gum} calculated from 30-hr (full-scale) Cp time series for a certain combination of t_{pk_g} and n_{pk_g}
t_{total}	Total testing time required to estimate Cp_{pk_g}, which is (t_{pk_g} x n_{pk_g})
F_{emp}	Empirical cumulative distribution function
F_g	Gumbel modeled cumulative distribution function
F_{pk_frac}	Peak fractile level set for the estimated peak pressure coefficient
U_{pk_g}	95% probability range of all Cp_{pk_g} estimated for a certain combination of t_{pk_g} and n_{pk_g}
U_{emp}	Cp_{emp} +/- 3 standard error (S.E.) range
MSE	Mean square error between the individual estimated peaks (Cp_{pk_g}) and empirically estimated peak (Cp_{emp})
e	Difference between U_{pk_g} and U_{emp}

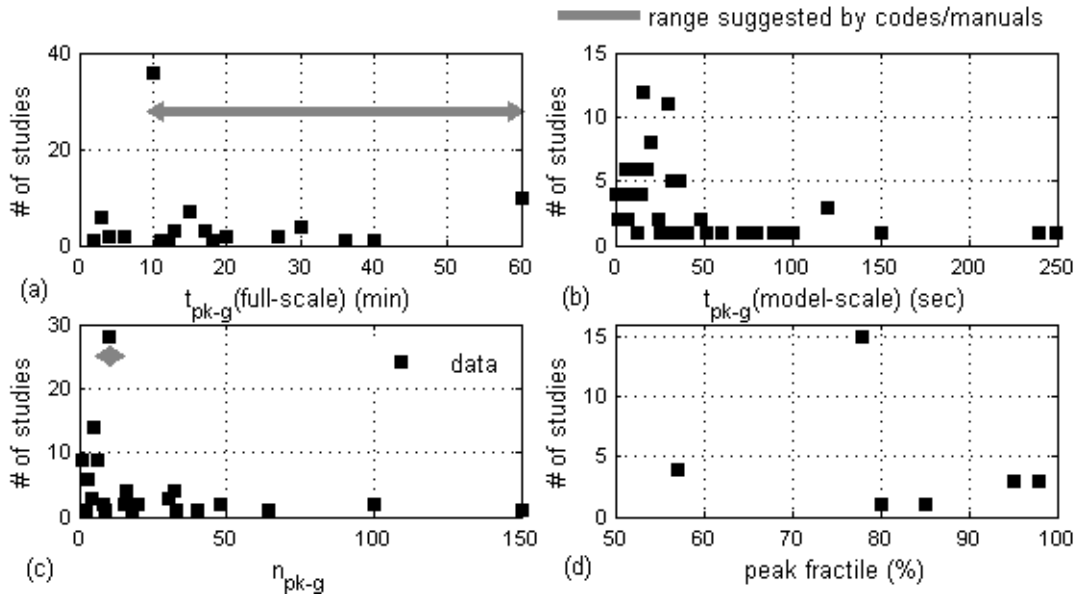

Fig. 1. Statistics of parameters for Gumbel fitting method utilized in previous studies: (a) peak sampling duration in full-scale, (b) peak sampling duration in model-scale, (c) number of peaks observed, (d) peak fractile level.

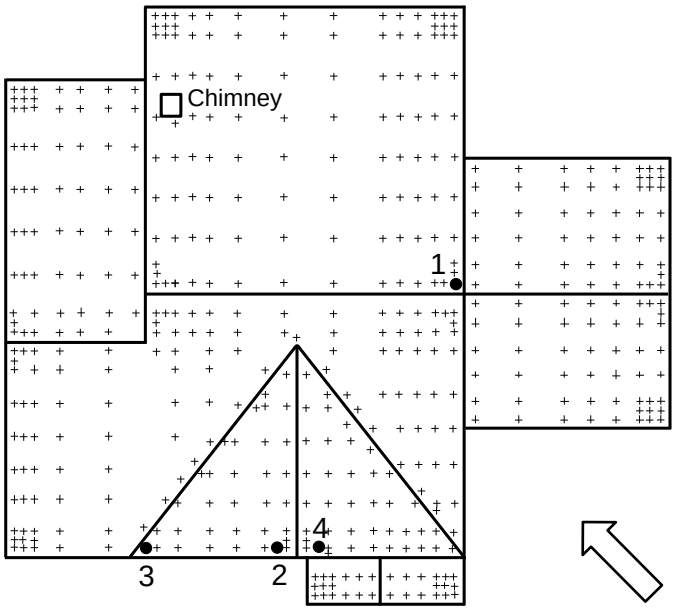

Fig. 2. Plan view of the building model, with the tap locations 1 – 4 indicated. The arrow indicates the wind direction used in the analysis.

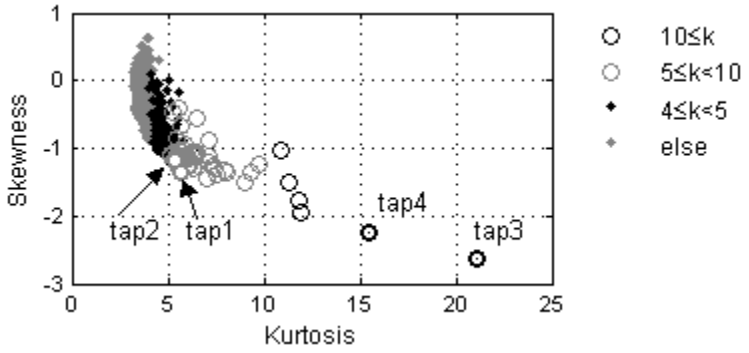

Fig. 3. Skewness and kurtosis pair of *Cp* data measured at 493 taps.

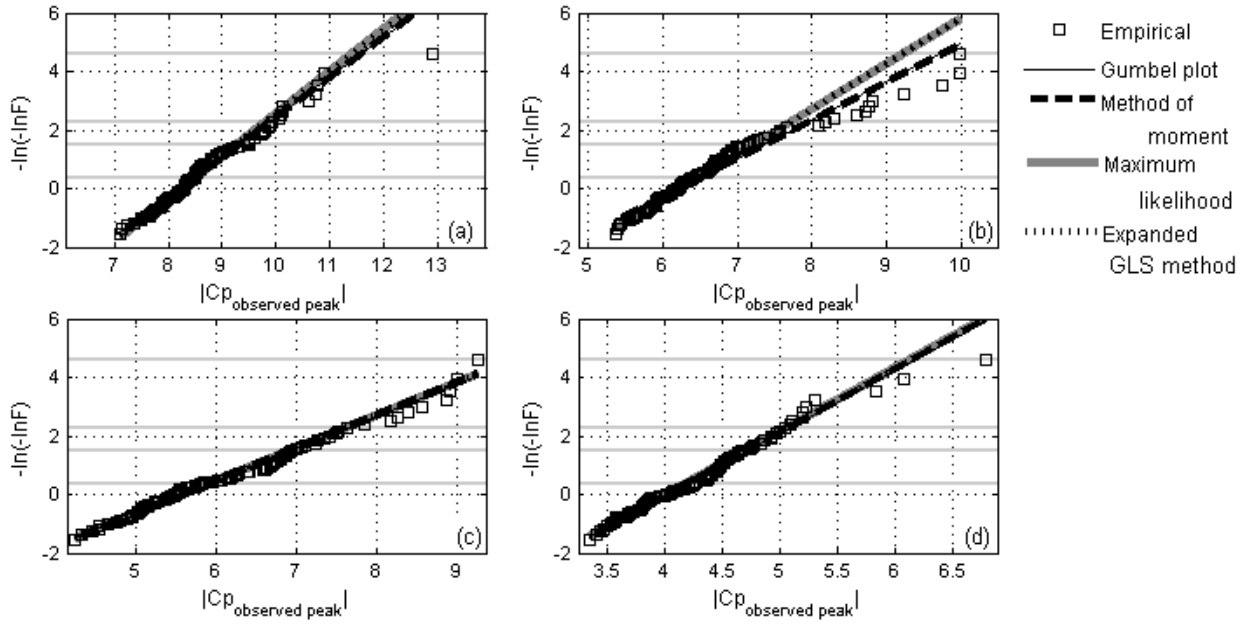

Fig. 4. Observed values of Cp_{pk_g} for t_{pk_g}=18 min & n_{pk_g}=100, as well as fits to the Gumbel distribution using several methods: (a) Tap 1, (b) Tap 2, (c) Tap3, and (d) Tap 4.

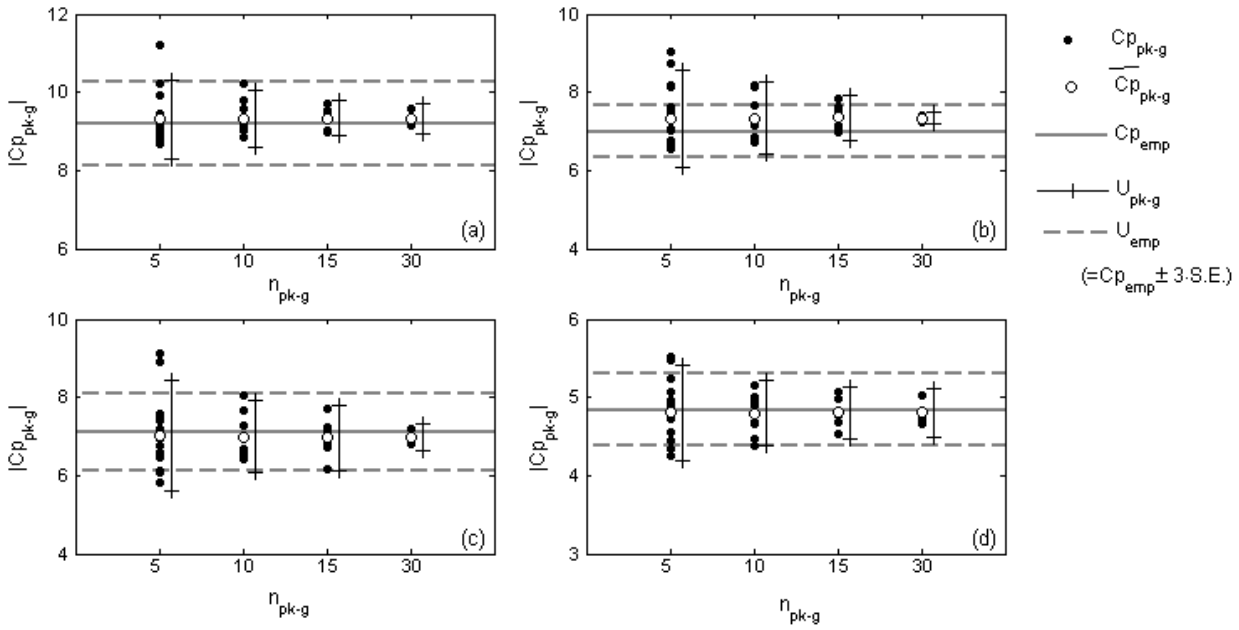

Fig. 5. Plots of Cp_{pk_g} for all n_{pk_g} with t_{pk_g} =20 min, from single tap Cp time histories at the 4 selected taps in Fig. 2: (a) Tap 1, (b) Tap 2, (c) Tap3, and (d) Tap 4. Values shown are the estimated values of Cp_{pk_g} (●) and its mean, $\overline{Cp}_{pk\_g}$ (○), and 95% probability range, U_{pk_g}, (+). Also included are the peak values from the empirical distribution, Cp_{emp} (solid gray line), and U_{emp} range (dashed gray line).

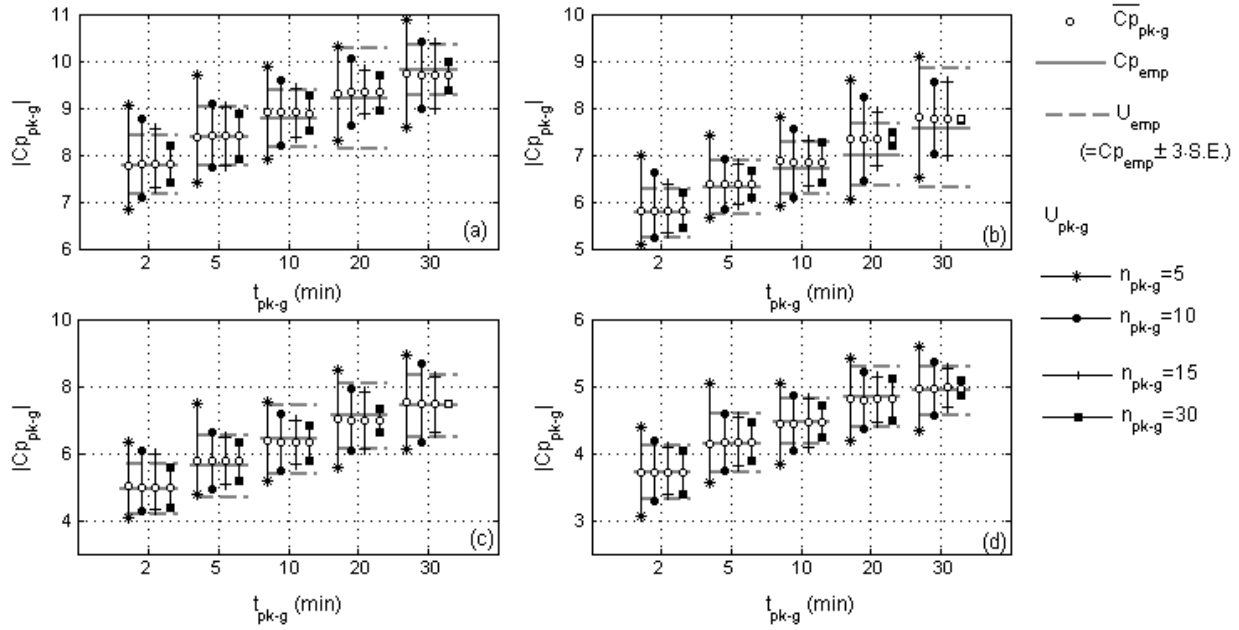

Fig. 6. Plots of Cp_{pk_g} for all n_{pk_g} and t_{pk_g}, from single tap Cp time histories at the 4 selected taps in Fig. 2: (a) Tap 1, (b) Tap 2, (c) Tap3, and (d) Tap 4. Values shown are the mean of the estimated peak, $\overline{Cp}_{pk\_g}$ (○), and 95% probability range, U_{pk_g}, (*, ●, +, ■). Also included are the peak values from the empirical distribution, Cp_{emp} (solid gray line), and U_{emp} range (dashed gray line).

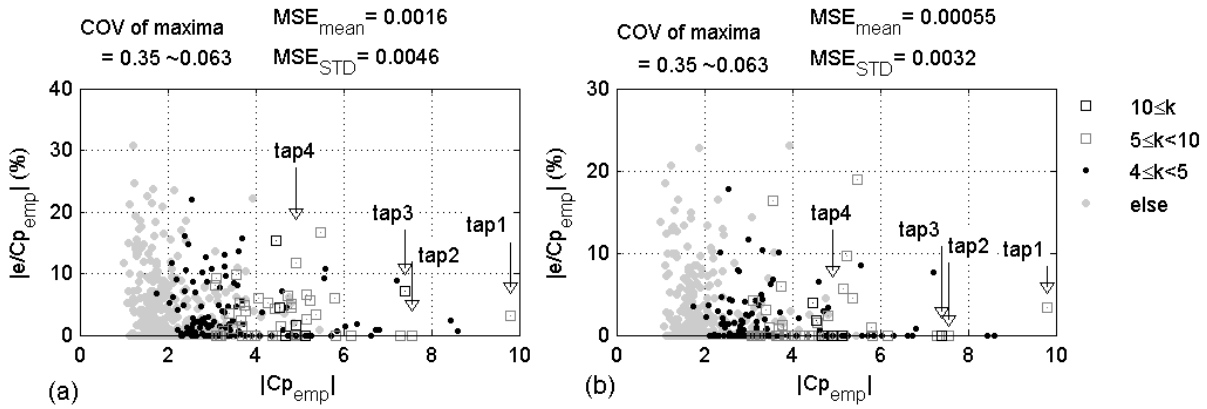

Fig. 7. Plots of peak values from the empirical distribution, Cp_{emp} (horizontal axis) and the difference between U_{pk_g} and U_{emp} divided by Cp_{emp} (vertical axis) for all 493 taps for t_{pk_g} =30 min: (b) n_{pk_g} =10, (c) n_{pk_g} =15.

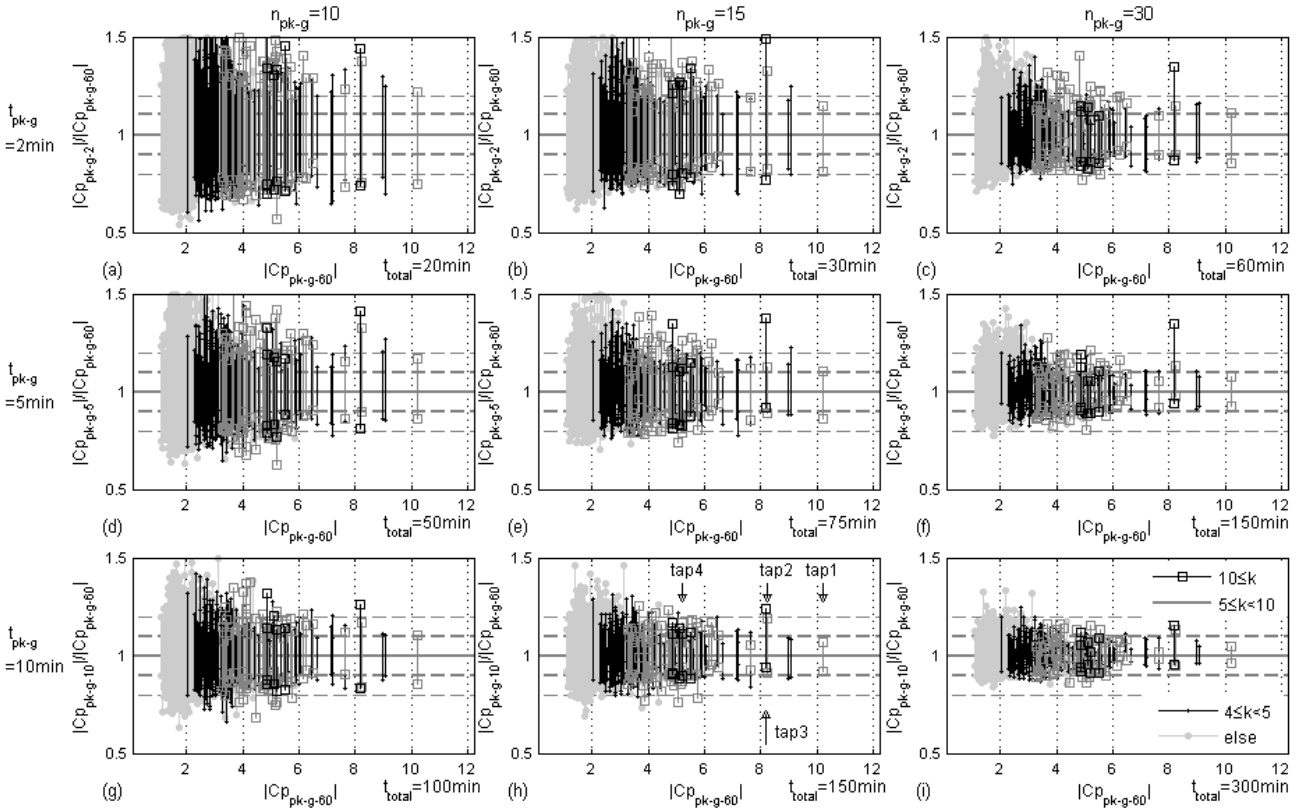

Fig. 8. Cp_{pk_g} values for t_{pk_g} = 60 min ("Cp_{pk_60}"), those for t_{pk_g} = 2, 5, and 10 min converted to 60 min using Eqs. (6) & (7) ("Cp_{pk_2}, Cp_{pk_5}, Cp_{pk_10}"), as well as the +/-10 and 20% ranges of estimated values (horizontal dashed gray lines).

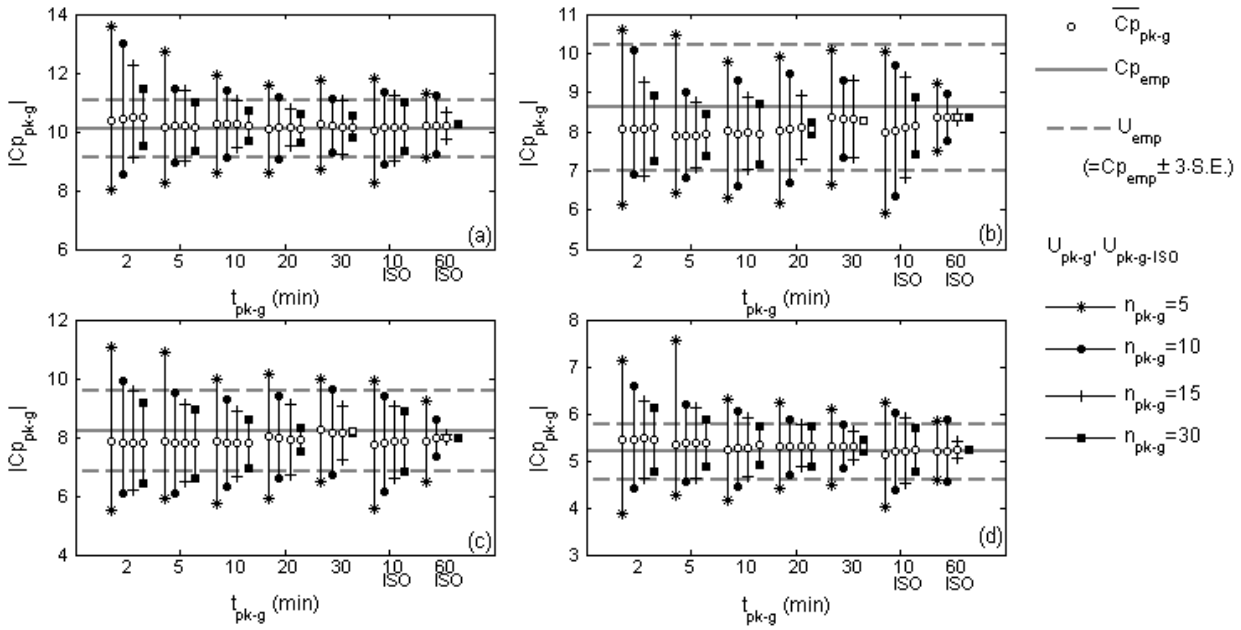

Fig. 9. Plots of Cp_{pk_g} for all n_{pk_g} and t_{pk_g}, from single tap Cp time histories at the 4 selected taps (Fig. 2) with conversion to t_{pk_g} =60 min using Eqs. (6) & (7): (a) Tap 1, (b) Tap 2, (c) Tap3, and (d) Tap 4. Values shown are the mean of the estimated peak, $\overline{Cp}_{pk\_g}$ (○), and 95% probability range, U_{pk_g}, (*, ●, +, ■). Also included are the peak values from the empirical distribution, Cp_{emp} (solid gray line), U_{emp} range (dashed gray line), and 95% probability range of ISO peaks calculated with t_{pk_g} =10 min and 60 min for various n_{pk_g}, $U_{pk\_g\_ISO}$.

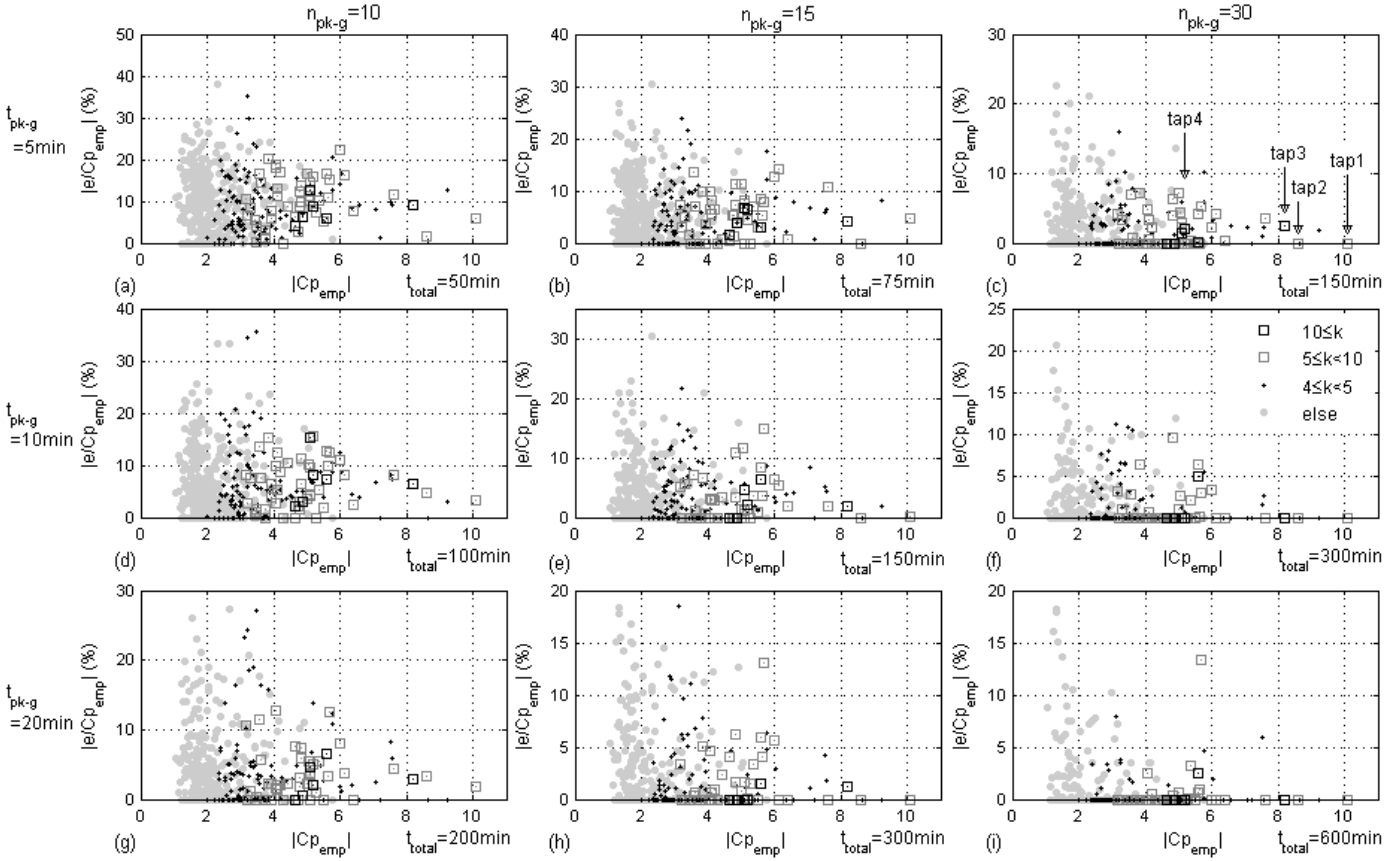

Fig. 10. Plots of peak values from the empirical distribution, Cp_{emp} (horizontal axis) and the difference between U_{pk_g} and U_{emp} divided by Cp_{emp} (vertical axis) for all 493 taps.

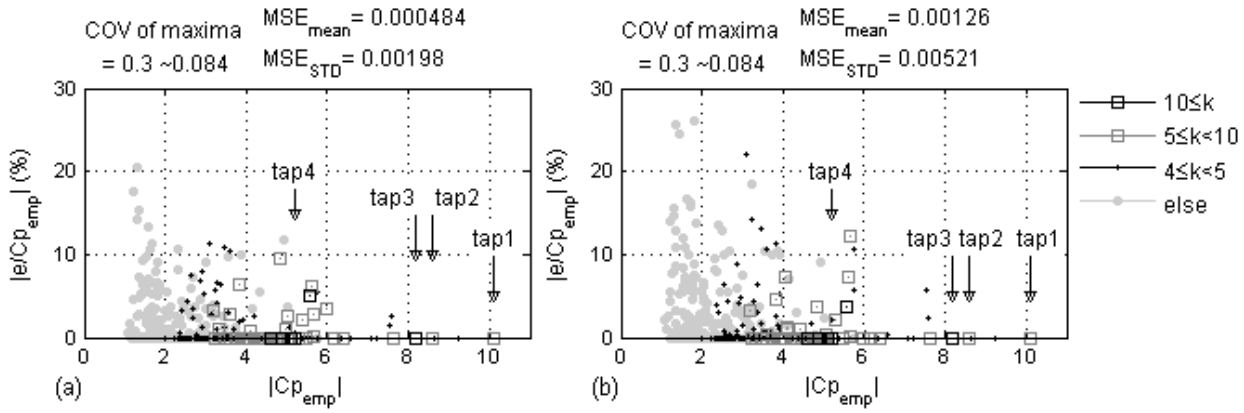

Fig. 11. Plots of peak values from the empirical distribution, Cp_{emp} (horizontal axis) and (a) the difference between U_{pk_g} and U_{emp} divided by Cp_{emp} (vertical axis) where U_{pk_g} calculated using Gumbel fitting approach for t_{pk_g} = 10 min & n_{pk_g} =30 converted to 60 min using Eqs. (6) & (7), and (b) the difference between $U_{pk\_g\_ISO}$ and U_{emp} divided by Cp_{emp} (vertical axis) where $U_{pk\_g\_ISO}$ calculated for t_{pk_g} = 10 min & n_{pk_g} =30 for all 493 taps in Fig. 2.

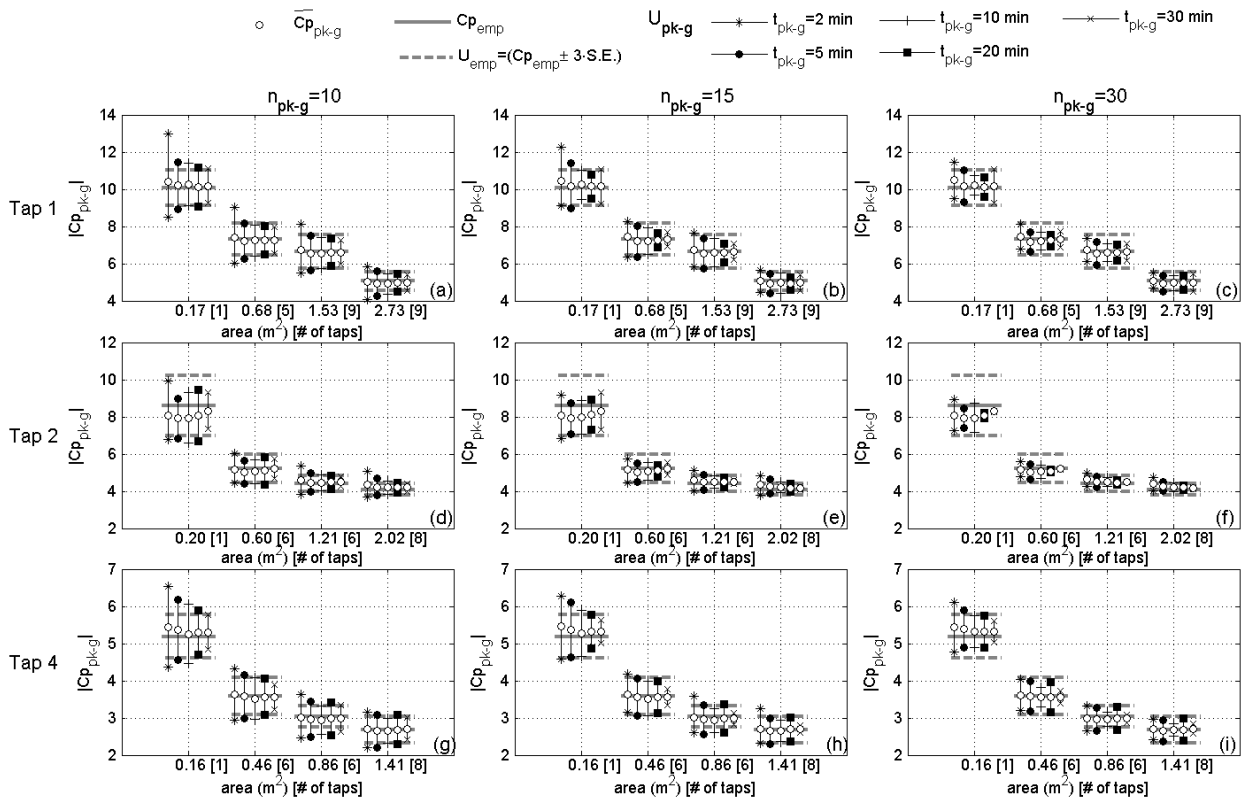

Fig. 12. Plots of Cp_{pk_g} for n_{pk_g} =10, 15, 30 and all t_{pk_g}, from area-averaged Cp histories at the 3 selected taps with conversion to t_{pk_g} =60 min using Eqs. (6) & (7).Values shown are the mean of the estimated peak, $\overline{Cp}_{pk\_g}$ (○), and 95% probability range, U_{pk_g}, (*, ●, +, ■, ×). Also included are the peak values from the empirical distribution, Cp_{emp} (solid gray line) and U_{emp} range (dashed gray line).